Journal of Geomatics Vol 12 No. 1 April 2018

Performance enhancement of Rational Function Model (RFM) for improved geo-position accuracy of IKONOS stereo satellite imagery

Tamer M. Saleh, Mohamed I. Zahran, Ayman R. El-Sheaby, and Mahmoud S. Gomaa
Department of Surveying Engineering, University of Benha, 108 Shoubra Street, Cairo, Egypt
Email: tamer.mohamed@feng.bu.edu.eg, mohamed.zahran01@feng.bu.edu.eg, ayman.alshehaby@feng.bu.edu.eg, mahmoud.goma@feng.bu.edu.eg

(Received: Oct 20, 2017; in final form: Apr 08, 2018)

Abstract: The RFM has been considered as a generic sensor model. Compared to the widely used polynomial models, RFM is essentially a more generic and expressive form. Utilizing the RFM to replace physical sensor models in photogrammetric mapping is becoming a standard way for economical and fast mapping from high-resolution imagery. This model uses the Rational Polynomial Coefficients (RPCs) supplied with the images, since IKONOS precise sensor and orbit parameters are not released by the satellite company. This paper presents three mathematical models for performance enhancement of RFM using IKONOS stereo satellite images, namely: 1) Bias-corrected image space; 2) Bias-corrected RPCs; and 3) Bias-corrected ground space. The three models were tested and compared with the well-known 3D-Affine and Direct Linear Transformation (DLT) models. The Least Squares Method (LSM) was applied to implement the different mathematical setups for estimating the correction parameters. Attained results show that the accuracies of the five models are slightly variant. With five GCPs, an accuracy of 0.8 m in X, 1.2 m in Y, and 1.3 m in height is achieved using the bias corrected image space and an accuracy of 0.9 m in X, 1 m in Y, and 1.6 m in height is reached using the bias corrected RPCs. On the other hand, the results indicate the effectiveness of 3D-Affine and DLT models especially when the RPCs and/or commercial software packages are not available for users.

Keywords: RFM, RPCs, Bias correction, 3D-Affine, DLT and Matlab.

1. Introduction

With the current growth in demand for high resolution satellite imagery (HRSI), great efforts have been made in natural hazards monitoring, resource management, change detection, planning, 3D shoreline extraction, DTM (Digital Terrain Model) and DSM (Digital Surface Model) generation (Poon et al., 2005; Xu et al., 2005; Di et al., 2003). A critical issue is the choice of a sensor model for HRSI to acquire high-accuracy 3D-reconstruction. In general, sensor models can be grouped into two classes, physical sensor models and generic sensor models. Physical sensor models are more rigorous and normally provide better accuracies since the model parameters employed represent the physical imaging process of sensors. However, building such physical sensor models requires information of the physical sensor and its imaging model. This information includes focal length, principal point location, pixel size, lens distortions and orientation parameters of the image. Collinear equations are rigorous models available for frame and push-broom sensors (Vincent and Yong, 2000). It is realized that this information is not always available, especially for images from commercial satellites. The generic sensor models are independent on sensor platforms as well as sensor types. Such properties have made generic sensor models very popular in the remote sensing community. The typical generic sensor models are polynomial-based ones (Vincent and Yong, 2000; Vincent and Yong, 2002). In terms of accuracy and computational stability, the bias compensation method (Fraser and Hanley, 2003) so far appears to be the best method and has been widely used (Fraser and Hanley, 2003, 2005; Hu et al., 2004). However, this method is effective only when the camera field of view (FOV) is narrow and the position and attitude errors are small (Grodecki and Dial, 2003).

Fraser and Hanley (2003) developed a method for the removal of exterior orientation biases in RPCs of IKONOS imagery. They found that only bias corrected RPCs of IKONOS is capable of generating accurate results with just one ground control point. Fraser and Hanley (2005) recognized the notable positioning accuracy attained with the RPC bundle adjustment with bias compensation. Furthermore, Fraser et al. (2006) gave an overview of the RPC model for high resolution satellite imagery, and highlighted the accuracy potential of RPC block adjustment. It has been demonstrated that bias compensated RPC block adjustment can yield sub-pixel positioning accuracy and highly accurate Ortho-images and digital surface models. Similar results were reported in Tong et al. (2010), which presented the two schemes: RPCs modification; and RPCs regeneration for orientation bias correction based on Quick-Bird stereo images in Shanghai. Four cases of bias correction were tested including: shift bias correction, shift and drift bias correction, affine model bias correction, and second-order polynomial bias correction. A least squares adjustment method is adopted for correction parameter estimation. The modified RPCs improve the accuracy from 23 m to 3 m in planimetry and from 17 m to 4 m in height. With the shift and drift bias correction method, the regenerated RPCs achieved a further improved positioning accuracy of 0.6 m in planimetry and 1 m in height with minimal two GCPs. The Rational Function Model (RFM) based on Rational Polynomial Coefficients (RPCs) is one of the generic models in use in place of rigorous models (Volpe and Rossi, 2003). After a rigorous sensor bundle adjustment is performed, multiple evenly distributed image/object grid points can be generated and used as ground control points (GCPs). Then, the RPCs are

calculated by these GCPs (Di et al., 2003). A least-squares method is used to estimate the RFM coefficients (RPCs) from a three-dimensional pseudo grid of points and orientation parameters. The RPCs are usually provided by imagery vendors of IKONOS, Quick-Bird, CARTOSAT – 1 etc. and were utilized for transformation from image to object space coordinates in a geographic reference system. Since sensor orientation is directly observed, there would be some systematic error in orientation parameters. Thus the refinement of RFM is required (Wu et al., 2008). In most studies mentioned above, biases in the image space or in the object space were modelled and corrected to refine RPCs-derived ground coordinates, while the original RPCs remained unchanged. Few studies were conducted to take the original set of coefficients from the RPC model and add new adjustable functions for both line and sample to the normal equations based on the known GCPs (Singh et al., 2008). For IKONOS stereo images, the sensor physical parameters are derived from the satellite ephemeris and attitude data without using GCPs. The satellite ephemeris data are determined using on-board Global Positioning System (GPS) receivers and sophisticated ground processing of the GPS data. The satellite attitude is determined by optimally combining star tracker data with measurements taken by the on-board gyros. Since the IKONOS satellite imagery vendor, Space Imaging Company, has not released the satellite ephemeris data, no physical mathematical model can be established. This causes a major problem in the process of geo-positioning from KONOS stereo imagery with high precision. Therefore, some generalized generic mathematical models are needed to substitute the physical models for IKONOS imagery restitution (Hu et al., 2004).

This paper deals with the biases in the RPC mapping due to the errors in sensor orientation. The performance of bias-corrected image space, bias-corrected RPCs and bias-corrected object space will be further investigated with IKONOS stereo-pair imagery. The main objective is to find the best set of parameters with least number of GCPs for RFM refinement. The models described in this paper were implemented through a prototype software developed by the authors in a Matlab environment. In addition, 3D Affine and DLT models are also applied and their accuracies are investigated for 3D positioning, compared with traditional and modified RFM.

The steps for RFM refinement using IKONOS stereo-pair imagery are similar to that using other types of stereo satellite images, which consist of, shown in figure 1.

- Affixing a set of distinct ground control and check points in the overlap area of the test image pair. The coordinates of those points are determined precisely by using static GPS positioning technique.
- Measuring the image coordinates of affixed control points in each of the two images of the test pair.
- Extracting the RPCs provided with the metadata files associated with the test image pair.
- Performing least-squares adjustment involving the provided RPCs and measured image coordinates of control points based on RFM as a mathematical model to get estimated coordinates of the control points.
- Assessing the accuracy of provided RPCs by computing the differences among measured and estimated coordinates of control points.
- Modelling biases are provided in RPCs by adding parameters to the traditional RFM , using different setups and different control configurations.
- Resolving the modified versions of RFM using least-squares method to get estimates for the added parameters associated with each version.
- Assessing the accuracy of modified RFM associated with each version by computing the differences among measured values of check points and their corresponding values estimated by the modified RFM.

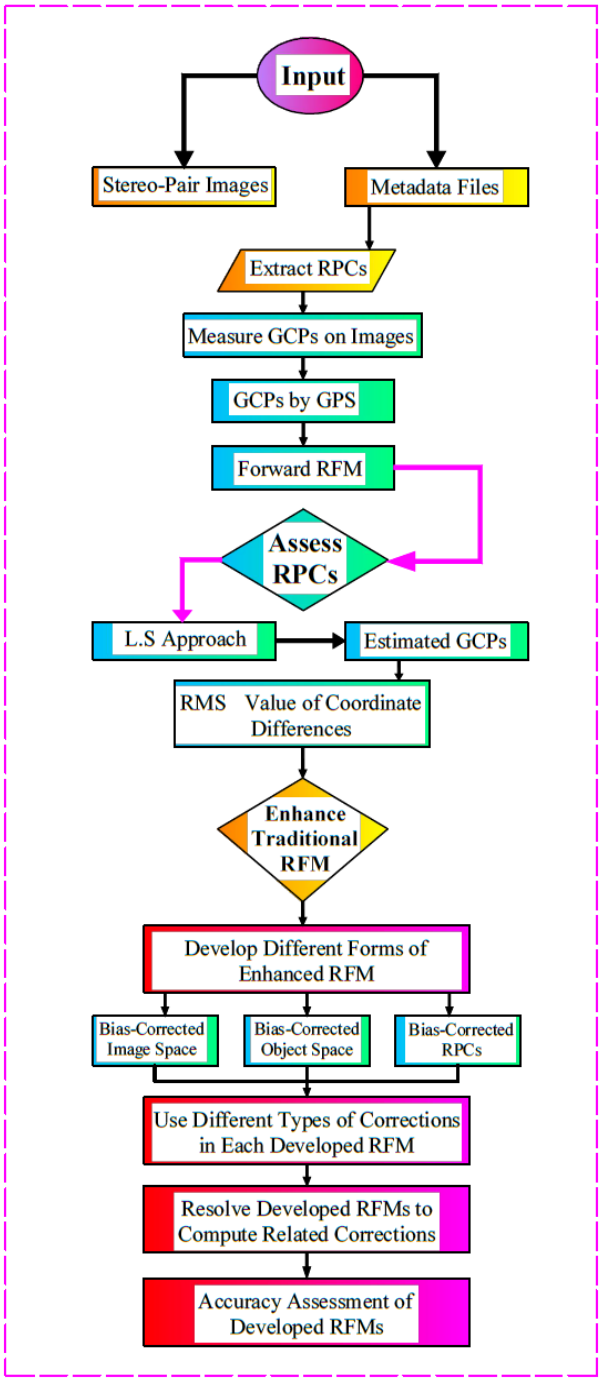

Figure 1: The strategy of developing the RF model

2. Mathematical models

2.1 Rational Function Model (RFM)

The RFM is one of the generic models that uses a ratio of two polynomial functions to compute the x and y coordinate in the image. The validation of this model has been tested in several researches with aerial photography data and satellite imageries (Tao et al., 2000). It takes the following general form (OGC, 1999):

$$l_n = \frac{\mathrm{P}_1\left(\mathrm{X_n}, \mathrm{Y_n}, \mathrm{Z_n}\right)}{\mathrm{P}_2\left(\mathrm{X_n}, \mathrm{Y_n}, \mathrm{Z_n}\right)} = \frac{\sum_{i=0}^{m_1}\sum_{j=0}^{m_2}\sum_{k=0}^{m_3} a_{\mathrm{ijk}} \mathrm{X}_n^i \mathrm{Y}_n^j \mathrm{Z}_n^k}{\sum_{i=0}^{n_1}\sum_{j=0}^{n_2}\sum_{k=0}^{n_3} b_{\mathrm{ijk}} \mathrm{X}_n^i \mathrm{Y}_n^j \mathrm{Z}_n^k}$$

$$s_n = \frac{\mathrm{P}_3\left(\mathrm{X_n}, \mathrm{Y_n}, \mathrm{Z_n}\right)}{\mathrm{P}_4\left(\mathrm{X_n}, \mathrm{Y_n}, \mathrm{Z_n}\right)} = \frac{\sum_{i=0}^{m_1}\sum_{j=0}^{m_2}\sum_{k=0}^{m_3} c_{\mathrm{ijk}} \mathrm{X}_n^i \mathrm{Y}_n^j \mathrm{Z}_n^k}{\sum_{i=0}^{n_1}\sum_{j=0}^{n_2}\sum_{k=0}^{n_3} d_{\mathrm{ijk}} \mathrm{X}_n^i \mathrm{Y}_n^j \mathrm{Z}_n^k} \quad (1)$$

Polynomial functions included in the model can be expressed as:

$$\begin{aligned}
\mathrm{P}_1\left(\mathrm{X_n}, \mathrm{Y_n}, \mathrm{Z_n}\right) &= a_0 + a_1 X_n + a_2 Y_n + a_3 Z_n + \ldots + a_{19} Z_n^3 \\
\mathrm{P}_2\left(\mathrm{X_n}, \mathrm{Y_n}, \mathrm{Z_n}\right) &= b_0 + \mathrm{b}_1 X_n + \mathrm{b}_2 Y_n + \mathrm{b}_3 Z_n + \ldots + \mathrm{b}_{19} Z_n^3 \\
\mathrm{P}_3\left(\mathrm{X_n}, \mathrm{Y_n}, \mathrm{Z_n}\right) &= c_0 + \mathrm{c}_1 X_n + \mathrm{c}_2 Y_n + \mathrm{c}_3 Z_n + \ldots + \mathrm{c}_{19} Z_n^3 \\
\mathrm{P}_4\left(\mathrm{X_n}, \mathrm{Y_n}, \mathrm{Z_n}\right) &= d_0 + \mathrm{d}_1 X_n + \mathrm{d}_2 Y_n + \mathrm{d}_3 Z_n + \ldots + \mathrm{d}_{19} Z_n^3
\end{aligned} \quad (2)$$

Where:

l_n, *and* s_n are the normalized line and sample coordinates in the image space. X_n,, Y_n, and Z_n are the normalized geodetic longitude, latitude and height in the object space. a_i, b_i, c_i *and* d_i are the polynomial coefficients RPCs (Total of 80). i, j and k are the increment values. m_1, m_2, m_3, n_1, n_2, n_3: are the order of the polynomial model (0-3), where $\mathrm{i} + \mathrm{j} + \mathrm{k} \leq 3$. The normalization of the coordinates is computed by (OGC, 1999):

$$l_n = \frac{\mathrm{Line} - \mathrm{Line\_OFF}}{\mathrm{Line\_Scale}} \; ; \; s_n = \frac{\mathrm{Sample} - \mathrm{Sample\_OFF}}{\mathrm{Sample\_Scale}} \quad (3)$$

$$\mathrm{X_n} = \frac{\lambda - \mathrm{Long\_OFF}}{\mathrm{Long\_Scale}} \; ; Y_n = \frac{\varphi - \mathrm{Lat\_OFF}}{\mathrm{Lat\_Scale}} \; ; \; \mathrm{Z_n} = \frac{h - \mathrm{Height\_OFF}}{\mathrm{Height\_Scale}}$$

Where Line and Sample are the image coordinates. Line_OFF and Sample_OFF are the offset values for the two image coordinates. Line_Scale and Sample_Scale are the scale factors for the two image coordinates. Similarly, $\boldsymbol{\varphi}$, $\boldsymbol{\lambda}$, and h are the geodetic latitude, longitude, and height in the object space. Lat_OFF, Long_OFF, and Height_OFF are the offset values for the three ground coordinates. Lat_Scale, Long_Scale, and Height_Scale are the corresponding scale factors.

2.1.1 3D-reconstruction using RFM

3D-reconstruction using various sensor models is one of the most important steps in accuracy assessment and enhancement of RPCs from IKONOS stereo-pair imagery. 3D-reconstruction could be achieved using the vendor-supplied RPCs. To assess the accuracy and bias distribution of the results using the raw RPCs, all the ground points (GPs) were used as check points (ChkPs). From the coordinates (l_n, s_n) in Equation (1), the following four equations can be derived for left (L) and right image (R):

$$\begin{aligned}
F_1 &= P_{1L}\left(\mathrm{X}_n, \mathrm{Y}_n, \mathrm{Z}_n\right) - l_{nL} P_{2L}\left(\mathrm{X}_n, \mathrm{Y}_n, \mathrm{Z}_n\right) = 0 \\
F_2 &= P_{3L}\left(\mathrm{X}_n, \mathrm{Y}_n, \mathrm{Z}_n\right) - s_{nL} P_{4L}\left(\mathrm{X}_n, \mathrm{Y}_n, \mathrm{Z}_n\right) = 0 \\
F_3 &= P_{1R}\left(\mathrm{X}_n, \mathrm{Y}_n, \mathrm{Z}_n\right) - l_{nR} P_{2R}\left(\mathrm{X}_n, \mathrm{Y}_n, \mathrm{Z}_n\right) = 0 \\
F_4 &= P_{3R}\left(\mathrm{X}_n, \mathrm{Y}_n, \mathrm{Z}_n\right) - s_{nR} P_{4R}\left(\mathrm{X}_n, \mathrm{Y}_n, \mathrm{Z}_n\right) = 0
\end{aligned} \quad (4)$$

Because of non-linearity of the equation and by applying the Taylor series expansion, the following equations are obtained (Grodecki et al., 2003):

$$\begin{aligned}
&\frac{\partial F_1}{\partial X_n}\Big|_0 dX_n + \frac{\partial F_1}{\partial Y_n}\Big|_0 dY_n + \frac{\partial F_1}{\partial Z_n}\Big|_0 dZ_n + \frac{\partial F_1}{\partial l_{nL}} V_{lnL} + \frac{\partial F_1}{\partial s_{nL}} V_{snL} = -F_1^0 \\
&\frac{\partial F_2}{\partial X_n}\Big|_0 dX_n + \frac{\partial F_2}{\partial Y_n}\Big|_0 dY_n + \frac{\partial F_2}{\partial Z_n}\Big|_0 dZ_n + \frac{\partial F_2}{\partial l_{nL}} V_{lnL} + \frac{\partial F_2}{\partial s_{nL}} V_{snL} = -F_2^0 \\
&\frac{\partial F_3}{\partial X_n}\Big|_0 dX_n + \frac{\partial F_3}{\partial Y_n}\Big|_0 dY_n + \frac{\partial F_3}{\partial Z_n}\Big|_0 dZ_n + \frac{\partial F_3}{\partial l_{nR}} V_{\mathrm{lnR}} + \frac{\partial F_3}{\partial s_{nR}} V_{snR} = -F_3^0 \\
&\frac{\partial F_4}{\partial X_n}\Big|_0 dX_n + \frac{\partial F_4}{\partial Y_n}\Big|_0 dY_n + \frac{\partial F_4}{\partial Z_n}\Big|_0 dZ_n + \frac{\partial F_4}{\partial l_{nR}} V_{\mathrm{lnR}} + \frac{\partial F_4}{\partial s_{nR}} V_{snR} = -F_4^0
\end{aligned} \quad (5)$$

The equations can be described in a matrix form as follow (Ghilani and Wolf, 2006).

$$AX + BV = K \quad (6)$$

$$\begin{bmatrix}
\frac{\partial F_{11}}{\partial X_n^1} & \frac{\partial F_{11}}{\partial Y_n^1} & \frac{\partial F_{11}}{\partial Z_n^1} & \ldots & 0 & 0 & 0 \\
\frac{\partial F_{21}}{\partial X_n^1} & \frac{\partial F_{21}}{\partial Y_n^1} & \frac{\partial F_{21}}{\partial Z_n^1} & \ldots & 0 & 0 & 0 \\
\frac{\partial F_{31}}{\partial X_n^1} & \frac{\partial F_{31}}{\partial Y_n^1} & \frac{\partial F_{31}}{\partial Z_n^1} & \ldots & 0 & 0 & 0 \\
\frac{\partial F_{41}}{\partial X_n^1} & \frac{\partial F_{41}}{\partial Y_n^1} & \frac{\partial F_{41}}{\partial Z_n^1} & \ldots & 0 & 0 & 0 \\
\ldots & & & \ldots & & & \\
\ldots & & & \ldots & & & \\
\ldots & & & \ldots & & & \\
\ldots & & & \ldots & & & \\
0 & 0 & 0 & \ldots & \frac{\partial F_{1N}}{\partial X_n^N} & \frac{\partial F_{1N}}{\partial Y_n^N} & \frac{\partial F_{1N}}{\partial Z_n^N} \\
0 & 0 & 0 & \ldots & \frac{\partial F_{2N}}{\partial X_n^N} & \frac{\partial F_{2N}}{\partial Y_n^N} & \frac{\partial F_{2N}}{\partial Z_n^N} \\
0 & 0 & 0 & \ldots & \frac{\partial F_{3N}}{\partial X_n^N} & \frac{\partial F_{3N}}{\partial Y_n^N} & \frac{\partial F_{3N}}{\partial Z_n^N} \\
0 & 0 & 0 & \ldots & \frac{\partial F_{4N}}{\partial X_n^N} & \frac{\partial F_{4N}}{\partial Y_n^N} & \frac{\partial F_{4N}}{\partial Z_n^N}
\end{bmatrix}
\begin{bmatrix} dX_n^1 \\ dY_n^1 \\ dZ_n^1 \\ \vdots \\ dX_n^N \\ dY_n^N \\ dZ_n^N \end{bmatrix} +
\begin{bmatrix}
\frac{\partial F_{11}}{\partial l_{nL}^1} & \frac{\partial F_{11}}{\partial s_{nL}^1} & 0 & 0 & \ldots \\
\frac{\partial F_{21}}{\partial l_{nL}^1} & \frac{\partial F_{21}}{\partial s_{nL}^1} & 0 & 0 & \ldots \\
0 & 0 & \frac{\partial F_{31}}{\partial l_{nR}^1} & \frac{\partial F_{31}}{\partial s_{nR}^1} & \ldots \\
0 & 0 & \frac{\partial F_{41}}{\partial l_{nR}^1} & \frac{\partial F_{41}}{\partial s_{nR}^1} & \ldots \\
 & & \ldots & & \\
 & & \ldots & & \\
 & & \ldots & & \\
 & & \ldots & & \\
\ldots & \frac{\partial F_{1N}}{\partial l_{nL}^N} & \frac{\partial F_{1N}}{\partial s_{nL}^N} & 0 & 0 \\
\ldots & \frac{\partial F_{2N}}{\partial l_{nL}^N} & \frac{\partial F_{2N}}{\partial s_{nL}^N} & 0 & 0 \\
\ldots & 0 & 0 & \frac{\partial F_{3N}}{\partial l_{nR}^N} & \frac{\partial F_{3N}}{\partial s_{nR}^N} \\
\ldots & 0 & 0 & \frac{\partial F_{4N}}{\partial l_{nR}^N} & \frac{\partial F_{4N}}{\partial s_{nR}^N}
\end{bmatrix}
\begin{bmatrix} V_{\mathrm{ln}L}^1 \\ V_{snL}^1 \\ V_{\mathrm{ln}R}^1 \\ V_{snR}^1 \\ \vdots \\ V_{\mathrm{ln}L}^N \\ V_{snL}^N \\ V_{\mathrm{ln}R}^N \\ V_{snR}^N \end{bmatrix} =
\begin{bmatrix} -F_{11}^0 \\ -F_{21}^0 \\ -F_{31}^0 \\ -F_{41}^0 \\ \vdots \\ -F_{1N}^0 \\ -F_{2N}^0 \\ -F_{3N}^0 \\ -F_{4N}^0 \end{bmatrix} \quad (7)$$

The partial derivatives can be calculated similar to what follows (Xu et al., 2005):

$$\frac{\partial F_1}{\partial X_n}\Big|_0 = (a_{1L} - l_{nL}b_{1L}) + (a_{4L} - l_{nL}b_{4L})Y_n + (a_{5L} - l_{nL}b_{5L})Z_n + 2(a_{7L} - l_{nL}b_{7L})X_n + (a_{10L} - l_{nL}b_{10L})Y_nZ_n + 3(a_{11L} - l_{nL}b_{11L})X_n^2 + (a_{12L} - l_{nL}b_{12L})Y_n^2 + (a_{13L} - l_{nL}b_{13L})Z_n^2 + 2(a_{14L} - l_{nL}b_{14L})X_nY_n + 2(a_{17L} - l_{nL}b_{17L})X_nZ_n \quad (8)$$

The full set of unknowns in Equation (7) can be resolved by using the least squares adjustment method as follow:

$$X = \left(A^T\left(BB^T\right)^{-1}A\right)^{-1}\left(A^T\left(BB^T\right)^{-1}K\right) \quad (9)$$

$$V = \left(B^T\left(BB^T\right)^{-1}\right)(K - AX) \quad (10)$$

Where A is a (4*No. of GPs) * (3*No. of GPs) matrix. X is a (3*No. of GPs)* (1) unknown vector. B is a matrix of observations (4*No. of GPs) * (4*No. of GPs). V is the vector of residual errors (4*No. of GPs)* (1). K is an (4*No. of GPs) * (1) Absolute vector. (No. of GPs) is the number of ground control points selected by the user. The unknown object space coordinates are solved for iteratively. At the first iteration, initial values for coordinates are needed, which could be determined through linear equations such as 3D-Affine or DLT model.

2.2 RPCs refinement methods

The RPCs may be refined directly or indirectly. Direct refining methods calculate the RPCs and thus requires a large number (more than 39) of GCPs for the 3rd order RFM, while indirect refining methods introduce complementary transformations in image or object space, and do not change the original RPCs directly (Hu et al., 2004). In this research, indirect method is adopted using three different approaches, as described in the following subsections.

2.2.1 Bias-corrected image space

This bias correction method proposes a polynomial model defined in image space, in which Δl and Δs are added to the rational functions to capture the differences between the nominal and the measured image space coordinates (Fraser and Hanley, 2003; Grodecki and Dial, 2003). The following equations provide the form of the refined RFM using first order polynomials transformation (Hanley and Fraser, 2004):

$$l + \Delta l = \frac{P_1(X_n, Y_n, Z_n)}{P_2(X_n, Y_n, Z_n)} * \text{Line\_Scale} + \text{Line\_OFF}$$

$$s + \Delta s = \frac{P_3(X_n, Y_n, Z_n)}{P_4(X_n, Y_n, Z_n)} * \text{Sample\_Scale} + \text{Sample\_OFF} \quad (11)$$

Where l and s are line and sample coordinates; Δl and Δs represent the differences between the measured and the calculated line and sample coordinates, which can be generally described as polynomials of the image line and sample coordinates as follows (Grodecki and Dial, 2003; Gong and Fritsch, 2016):

$$\Delta l = A_0 + A_1 l + A_2 s + A_3 l^2 + A_4 l.s + A_5 s^2 + \ldots$$

$$\Delta s = B_0 + B_1 l + B_2 s + B_3 l^2 + B_4 l.s + B_5 s^2 + \ldots \quad (12)$$

Where A_i and B_i (i = 1, 2, 3, …) are the correction parameters. By using affine transformation, sub-pixel accuracy can be obtained (Fraser and Hanley, 2003. However, the method is effective only when the camera FOV is narrow and the position and attitude errors are small (Grodecki and Dial, 2003).

In view of the high-order dynamic characteristic of the IKONOS sensor, three comparative choices of correction parameters are tested in this research: 1) A_0, A_1, B_0, B_1 which models the shift and scale; 2) A_0, A_1, A_2, B_0, B_1, B_2 which models the bias using the entire transformation model; 3) $A_0 \approx A_5$, $B_0 \approx B_5$ which models the bias using second-order polynomials. This model is used to check whether distinct high order errors exist in IKONOS imaging orientation.

With an adequate provision of GCPs, the correction parameters are estimated by using the LSM. First, using the original vendor provided RPCs and measured object coordinates of control points based on RFM as a mathematical model to get the calculated image space (l_c, s_c) potentially containing inherent biases. The calculated image coordinates are compared with the measured image coordinates (l_m, s_m) to obtain the residuals (Δl, Δs). After that, the correction parameters are further computed based on the discrepancies on all the image control points using the LSM. For clarity, assume that 4 GCPs exist for the affine parameter estimation. The observation equations (AX + BV = K) can be described in a matrix form as follow;

$$\begin{bmatrix} \frac{\partial F_{11}}{\partial A_{0L}} & \frac{\partial F_{11}}{\partial A_{1L}} & \frac{\partial F_{11}}{\partial A_{2L}} & 0\ 0\ 0 \\ 0\ 0\ 0 & \frac{\partial F_{21}}{\partial B_{0L}} & \frac{\partial F_{21}}{\partial B_{1L}} & \frac{\partial F_{21}}{\partial B_{2L}} \\ \frac{\partial F_{12}}{\partial A_{0L}} & \frac{\partial F_{12}}{\partial A_{1L}} & \frac{\partial F_{12}}{\partial A_{2L}} & 0\ 0\ 0 \\ 0\ 0\ 0 & \frac{\partial F_{22}}{\partial B_{0L}} & \frac{\partial F_{22}}{\partial B_{1L}} & \frac{\partial F_{22}}{\partial B_{2L}} \\ \frac{\partial F_{13}}{\partial A_{0L}} & \frac{\partial F_{13}}{\partial A_{1L}} & \frac{\partial F_{13}}{\partial A_{2L}} & 0\ 0\ 0 \\ 0\ 0\ 0 & \frac{\partial F_{23}}{\partial B_{0L}} & \frac{\partial F_{23}}{\partial B_{1L}} & \frac{\partial F_{23}}{\partial B_{2L}} \end{bmatrix} \begin{bmatrix} A_{0L} \\ A_{1L} \\ A_{2L} \\ B_{0L} \\ B_{1L} \\ B_{2L} \end{bmatrix} + \begin{bmatrix} \frac{\partial F_{11}}{\partial l_{nL}^1} & 0 & 0 & 0 & 0 & 0 \\ 0 & \frac{\partial F_{21}}{\partial s_{nL}^1} & 0 & 0 & 0 & 0 \\ 0 & 0 & \frac{\partial F_{12}}{\partial l_{nL}^2} & 0 & 0 & 0 \\ 0 & 0 & 0 & \frac{\partial F_{22}}{\partial s_{nL}^2} & 0 & 0 \\ 0 & 0 & 0 & 0 & \frac{\partial F_{13}}{\partial l_{nL}^3} & 0 \\ 0 & 0 & 0 & 0 & 0 & \frac{\partial F_{23}}{\partial s_{nL}^3} \end{bmatrix} \begin{bmatrix} V_{\ln L}^1 \\ V_{\text{sn}L}^1 \\ V_{\ln L}^2 \\ V_{\text{sn}L}^2 \\ V_{\ln L}^3 \\ V_{\text{sn}L}^3 \end{bmatrix} = \begin{bmatrix} -F_{11}^0 \\ -F_{21}^0 \\ -F_{12}^0 \\ -F_{22}^0 \\ -F_{13}^0 \\ -F_{23}^0 \end{bmatrix} \quad (13)$$

The six affine parameters in Equation (12) can be resolved by using the LSM, described in Equation (9). If the shift and scale bias [A_0, A_1, B_0, *and* $B1$] are the only factors taken into account, the correction can be made by improving the original RPCs. As detailed in Fraser and Hanley (2003 and 2005), only the parameters in numerator need to be updated, and the refined RPC model becomes:

$$l_n = \frac{(a_0 - b_0\Delta l_n) + (a_1 - b_1\Delta l_n)X_n + \ldots + (a_{19} - b_{19}\Delta l_n)Z_n^3}{P_2(X_n, Y_n, Z_n)}$$

$$s_n = \frac{(c_0 - d_0\Delta s_n) + (c_1 - d_1\Delta s_n)X_n + \ldots + (c_{19} - d_{19}\Delta s_n)Z_n^3}{P_4(X_n, Y_n, Z_n)} \quad (14)$$

Where a_i, b_i, c_i, and d_i are the original vendor-provided RPCs, Δl_n and Δs_n are the normalized values of the image shift and scale bias parameters Δl and Δs.

Effectively, all original terms in the numerator of each expression in Equation (11) are modified; each coefficient a_i is replaced by $(a_i - b_i\ \Delta l_n)$. In this way, the vendor-supplied RPCs can be replaced using the method mentioned above. The bias inside the initial RPCs could be corrected. This would be much more convenient for some digital photogrammetric software packages such as IMAGINE Photogrammetry, which only support the use of RPCs to do the 3D-reconstruction of IKONOS imagery (Xu et al., 2005). Figure 2 shows the 3D-reconstruction steps when using updated RPCs:

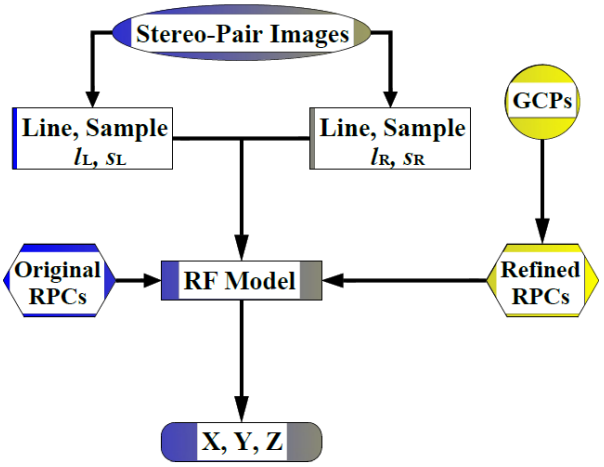

Figure 2: Steps of 3D-reconstruction using updated RPCs

2.2.2 Bias-corrected RPCs

This approach is implemented by adding a set of new adjustable functions ΔN (numerator coefficient) and ΔD (denominator coefficient) for both line and sample equations based on the known GCPs to correct the RPCs (Singh et al., 2008). The new adjustable functions can be defined as follows:

$$l_n = \frac{P_1(X_n, Y_n, Z_n) + \Delta P_1}{P_2(X_n, Y_n, Z_n) + \Delta P_2}$$

$$s_n = \frac{P_3(X_n, Y_n, Z_n) + \Delta P_3}{P_4(X_n, Y_n, Z_n) + \Delta P_4} \quad (15)$$

ΔP_1, ΔP_2, ΔP_3, and ΔP_4 are the differences between the original and the adjustable, which can be generally described as (Singh et al., 2008):

$$\begin{aligned}
\Delta P_1 &= A_0 + A_1 X_n + A_2 Y_n + A_3 Z_n + \ldots + A_{19} Z_n^3 \\
\Delta P_2 &= B_0 + B_1 X_n + B_2 Y_n + B_3 Z_n + \ldots + B_{19} Z_n^3 \\
\Delta P_3 &= C_0 + C_1 X_n + C_2 Y_n + C_3 Z_n + \ldots + C_{19} Z_n^3 \\
\Delta P_4 &= D_0 + D_1 X_n + D_2 Y_n + D_3 Z_n + \ldots + D_{19} Z_n^3
\end{aligned} \quad (16)$$

A_i, B_i, C_i and D_i are the correction parameters in the correction model. The resulted estimates of correction parameters are added to the original coefficients to get refined RPCs. The correction parameters are further computed based on the control points using the LSM. For clarity, assume that 3 GCPs are used for estimation of the shift parameters (A_0, B_0, C_0, and D_0) for both left and right images. As a result, 12 observation equations in 8 unknowns are yielded. They can be described as in Equation (17). The unknown shift parameters can be resolved by using the LSM, utilizing Equation (9).

$$\begin{bmatrix}
\frac{\partial F_{11}}{\partial A_{0L}} & \frac{\partial F_{11}}{\partial B_{0L}} & 0 & 0 & 0 & 0 & 0 & 0 \\
0 & 0 & \frac{\partial F_{21}}{\partial C_{0L}} & \frac{\partial F_{21}}{\partial D_{0L}} & 0 & 0 & 0 & 0 \\
0 & 0 & 0 & 0 & \frac{\partial F_{31}}{\partial A_{0R}} & \frac{\partial F_{31}}{\partial B_{0R}} & 0 & 0 \\
0 & 0 & 0 & 0 & 0 & 0 & \frac{\partial F_{41}}{\partial C_{0R}} & \frac{\partial F_{41}}{\partial D_{0R}} \\
\frac{\partial F_{12}}{\partial A_{0L}} & \frac{\partial F_{12}}{\partial B_{0L}} & 0 & 0 & 0 & 0 & 0 & 0 \\
0 & 0 & \frac{\partial F_{22}}{\partial C_{0L}} & \frac{\partial F_{22}}{\partial D_{0L}} & 0 & 0 & 0 & 0 \\
0 & 0 & 0 & 0 & \frac{\partial F_{32}}{\partial A_{0R}} & \frac{\partial F_{32}}{\partial B_{0R}} & 0 & 0 \\
0 & 0 & 0 & 0 & 0 & 0 & \frac{\partial F_{42}}{\partial C_{0R}} & \frac{\partial F_{42}}{\partial D_{0R}} \\
\frac{\partial F_{13}}{\partial A_{0L}} & \frac{\partial F_{13}}{\partial B_{0L}} & 0 & 0 & 0 & 0 & 0 & 0 \\
0 & 0 & \frac{\partial F_{23}}{\partial C_{0L}} & \frac{\partial F_{23}}{\partial D_{0L}} & 0 & 0 & 0 & 0 \\
0 & 0 & 0 & 0 & \frac{\partial F_{33}}{\partial A_{0R}} & \frac{\partial F_{33}}{\partial B_{0R}} & 0 & 0 \\
0 & 0 & 0 & 0 & 0 & 0 & \frac{\partial F_{43}}{\partial C_{0R}} & \frac{\partial F_{43}}{\partial D_{0R}}
\end{bmatrix}
\begin{bmatrix} A_{0L} \\ B_{0L} \\ C_{0L} \\ D_{0L} \\ A_{0R} \\ B_{0R} \\ C_{0R} \\ D_{0R} \end{bmatrix}
+
\begin{bmatrix}
\frac{\partial F_{11}}{\partial l_{nL}^1} & 0 & 0 & 0 & 0 & 0 & 0 & 0 & 0 & 0 \\
0 & \frac{\partial F_{21}}{\partial s_{nL}^1} & 0 & 0 & 0 & 0 & 0 & 0 & 0 & 0 \\
0 & 0 & \frac{\partial F_{31}}{\partial l_{nR}^1} & 0 & 0 & 0 & 0 & 0 & 0 & 0 \\
0 & 0 & 0 & \frac{\partial F_{41}}{\partial s_{nR}^1} & 0 & 0 & 0 & 0 & 0 & 0 \\
0 & 0 & 0 & 0 & \frac{\partial F_{12}}{\partial l_{nL}^2} & 0 & 0 & 0 & 0 & 0 \\
0 & 0 & 0 & 0 & 0 & \frac{\partial F_{22}}{\partial s_{nL}^2} & 0 & 0 & 0 & 0 \\
0 & 0 & 0 & 0 & 0 & 0 & \frac{\partial F_{32}}{\partial l_{nR}^2} & 0 & 0 & 0 \\
0 & 0 & 0 & 0 & 0 & 0 & 0 & \frac{\partial F_{42}}{\partial s_{nR}^2} & 0 & 0 \\
0 & 0 & 0 & 0 & 0 & 0 & 0 & 0 & \frac{\partial F_{13}}{\partial l_{nL}^3} & 0 \\
0 & 0 & 0 & 0 & 0 & 0 & 0 & 0 & 0 & \frac{\partial F_{23}}{\partial s_{nL}^3} \\
0 & 0 & 0 & 0 & 0 & 0 & 0 & 0 & \frac{\partial F_{33}}{\partial l_{nR}^3} & 0 \\
0 & 0 & 0 & 0 & 0 & 0 & 0 & 0 & 0 & \frac{\partial F_{43}}{\partial s_{nR}^3}
\end{bmatrix}
\begin{bmatrix}
V_{\ln L}^1 \\ V_{\mathrm{sn}L}^1 \\ V_{\ln R}^1 \\ V_{\mathrm{sn}R}^1 \\ V_{\ln L}^2 \\ V_{\mathrm{sn}L}^2 \\ V_{\ln R}^2 \\ V_{\mathrm{sn}R}^2 \\ V_{\ln L}^3 \\ V_{\mathrm{sn}L}^3 \\ V_{\ln R}^3 \\ V_{\mathrm{sn}R}^3
\end{bmatrix}
=
\begin{bmatrix}
-F_{11}^0 \\ -F_{21}^0 \\ -F_{31}^0 \\ -F_{41}^0 \\ -F_{12}^0 \\ -F_{22}^0 \\ -F_{32}^0 \\ -F_{42}^0 \\ -F_{13}^0 \\ -F_{23}^0 \\ -F_{33}^0 \\ -F_{43}^0
\end{bmatrix}^a \quad (17)$$

Where 1, 2, and 3 in a matrix form are the number of control points.

2.2.3 Bias-corrected ground space

A polynomial model defined in the domain of object space to correct the ground coordinates derived from the vendor-provided RPCs as in Equation (18) (Di et al., 2003; Zhen Xiong and Yun Zhang, 2009). In this method, the polynomial correction parameters are determined by the GCPs as follows:

$$\begin{aligned}
X^{GPS} &= a_0 + a_1 X^{RF} + a_2 Y^{RF} + a_3 Z^{RF} \\
Y^{GPS} &= b_0 + b_1 X^{RF} + b_2 Y^{RF} + b_3 Z^{RF} \\
Z^{GPS} &= c_0 + c_1 X^{RF} + c_2 Y^{RF} + c_3 Z^{RF}
\end{aligned} \quad (18)$$

Where X^{GPS}, Y^{GPS}, Z^{GPS} are the observed ground coordinates; X^{RF}, Y^{RF}, Z^{RF} are the ground coordinates derived from the RPC; and a_i, b_i, c_i are the correction parameters.

2.3 Affine model

Since 2D Polynomial models do not take into account the heights of the GCPs, these models can be efficiently used when the image is not influenced by the topographic effects. In this case, low order polynomials can provide accurate results. The model can be represented as follow:

$$x = a_0 + a_1X + a_2Y$$
$$y = b_0 + b_1X + b_2Y \quad (19)$$

Where x, y are the image coordinates; X, Y are the 2D ground coordinates; and a_0, a_1, a_2, b_0, b_1, b_2 are polynomial coefficients. Some studies have shown that the use of low-order polynomial 3D models for images of hilly and mountainous areas can reach the accuracy level that is close to the rigorous models (Fraser et al., 1999). A typical formula can be expressed as follow:

$$x = a_0 + a_1X + a_2Y + a_3Z + a_4XY + a_5YZ + a_6XZ$$
$$y = b_0 + b_1X + b_2Y + b_3Z + b_4XY + b_5YZ + b_6XZ \quad (20)$$

Where X, Y, Z are the 3D ground coordinates.

2.4 Direct Linear Transformation (DLT) model

The DLT model was developed by Abdel Aziz and Karara (1971) for close range photogrammetry applications and can also be used for image rectification (Vincent and Yong, 2000). The DLT represents a special case of the RF Model, with first degree polynomials and common denominators:

$$x = \frac{L_1X + L_2Y + L_3Z + L_4}{L_9X + L_{10}Y + L_{11}Z + 1}$$
$$y = \frac{L_5X + L_6Y + L_7Z + L_8}{L_9X + L_{10}Y + L_{11}Z + 1} \quad (21)$$

Where x, y are the image coordinates; X, Y, Z are the ground coordinates; and L_1, L_2, L_3, L_4, L_5, L_6, L_7, L_8, L_9, L_{10} and L_{11} are polynomial coefficients.

3. Study area and dataset

A Pan-sharpened stereo pair of IKONOS imagery, for an area in the *north of Khartoum in Sudan* about 16 km north of *Omdurman city* is obtained by the Edge Pro Company. The study area covers almost 5.8 km x 5.3 km. It includes various topographic features, urban area, hilly terrain and a part of *Wadi Sayidna Air Base* as shown in figure 3. It was the first stereo pair of IKONOS images acquired over Sudan in December 27, 2003. The data are delivered in Geo-Tiff format with text files containing the rational polynomial coefficients (RPCs) for each image. Table 1 shows the main parameters of the stereo-pairs.

A set of 21 well-identified and well distributed points on the images were selected. Mostly corners of buildings and fences/walls as well as road intersections were selected and surveyed using GPS in a static mode with about 5 mm accuracy. Leica Geo-office software was used to process the data with survey positions being referenced to the UTM/WGS84 zone 36N. Corresponding image coordinates on both the left and right image of the stereo-pair were measured in the IMAGINE photogrammetry software. Figure 4 shows the distribution of the GPS points; GCP environment in red and ChkPs in green.

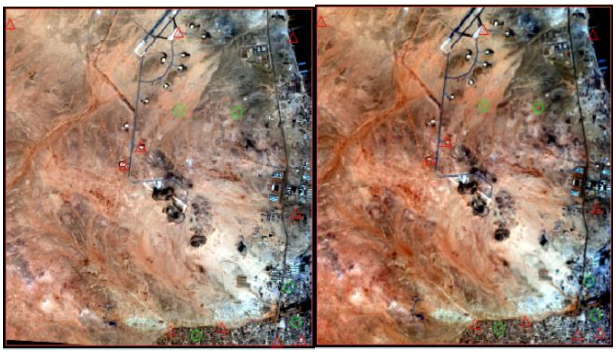

Figure 3: Stereo IKONOS image for the study area

Table 1: Main parameters of the available IKONOS HRSI 1 m stereo-pair

Acquisition Date / Time	08:41 GMT 27-12-2003 and 08:42 GMT 27-12-2003
Sun Angle Azimuth	156.1241 and156.3809 degrees
Sun Angle Elevation	63.50707 and 47.50945 degrees
Overlap	99%
Rows	5893 and 6004 pixels
Columns	5351 and 5357 pixels
Pixel Size	1.000 meters
Percent Component Cloud Cover	0

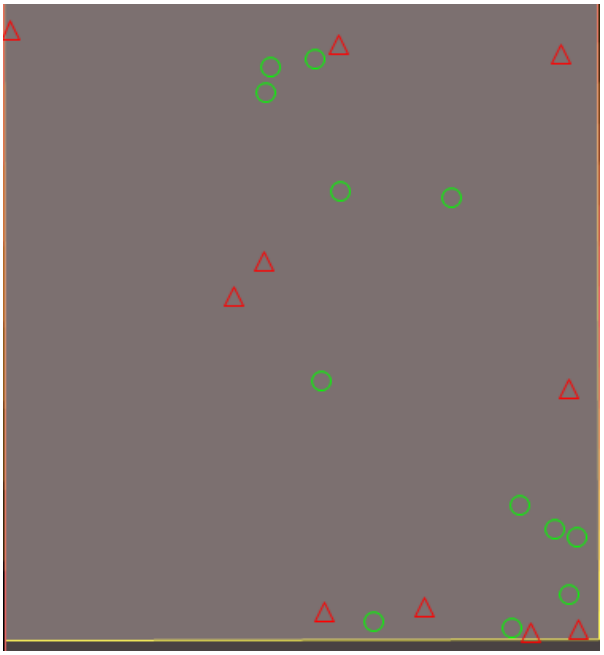

Figure 4: GCPs and ChkPs distribution

4. Results and analysis

Several experiments were performed to apply the described mathematical models. Before testing and evaluating those models, the accuracy of the acquired IKONOS images was checked by locating the twenty one GCPs on the images, estimating their ground coordinates using RFM and comparing estimated coordinates to known coordinates. The results show that the RMS value of differences in X, Y and Z were 7.2 m, 3.1 m, and 16.7 m respectively.

4.1 Performance evaluation of RFM

In the first experiment, the 3D-reconstruction has been achieved using the vendor-supplied RPCs. To assess the accuracy and bias distribution of the results using the raw RPCs, all the 21 ground points were used as ChkPs. The RMS value of differences between known and estimated coordinates were calculated and listed in table 2 which significantly indicate the existence of large shift bias. Figure 5 shows the planimetric and vertical accuracies at ChkPs based on vendor-supplied RPCs and figure 6 shows bias vectors of left and right image at the same points.

Table 2: RMS value for ChkPs using RPCs without GCPs

Statistic	RMS of check points coordinate differences (meters)		
	ΔX	ΔY	ΔZ
RMS	7.2	3.1	16.7

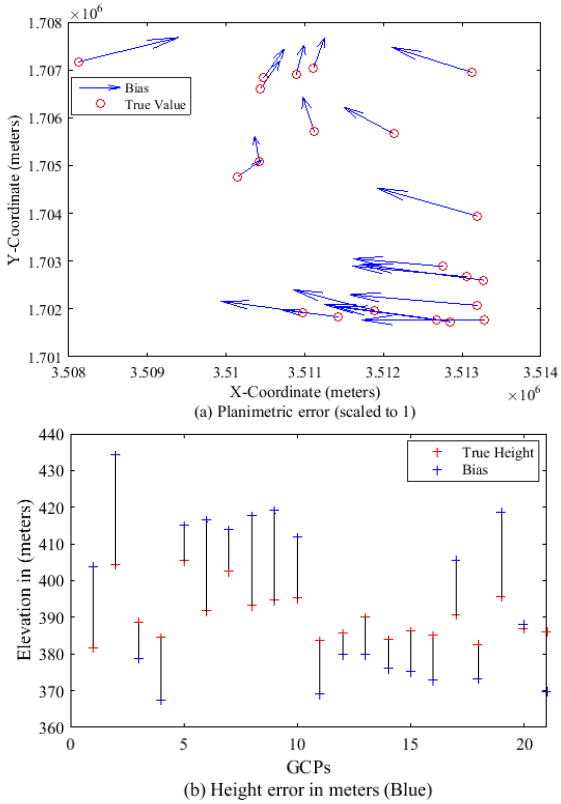

Figure 5: Bias vectors of (a) planimetry and (b) elevation at ChkPs based on vendor-supplied RPCs

4.2 Bias-corrected image space

The refined RFM in image space was applied using the IKONOS stereo images. Tables 3, 4 and 5 list the RMS value for the 18 ChkPs in the object space, which implement the refined model with polynomial transformation and different numbers of GCPs. Compared with the case without any GCPs, the results are significantly improved. It is clear that increasing the GCPs from 3 to 17 points does not improve much the accuracy. Therefore, five control points were sufficient to compensate for the shift and scale bias correction. Detailed discussions on the result of each correction model are given below:

4.2.1 Modelling with shift and scale

In shift and scale bias correction with all GCPs being employed (A_0, A_1, B_0, B_1), the biases in the object space are listed in table 3. To be more circumspect, the 1st order and 2nd order polynomials for the bias correction were further examined.

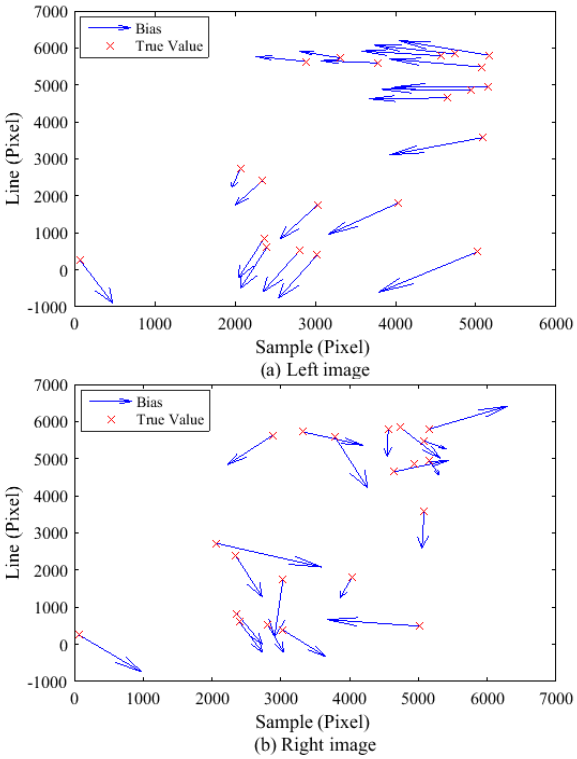

Figure 6: Bias vectors of (a) left and (b) right image at ChkPs, calculated using vendor-supplied RPCs

Table 3: RMS value of ChkPs using different selection of GCPs with shift and scale bias correction model

No. of GCPs/ChkPs	RMS of check points coordinate differences (meters)		
	X	Y	Z
3/18	2.4	1.0	1.2
5/16	0.9	1.0	1.6
7/14	0.9	0.9	1.7
9/12	1.0	1.0	1.8
13/8	0.3	1.0	1.5
15/6	0.3	0.6	1.5
17/4	0.3	0.6	1.2

4.2.2 Modelling with 1st order polynomial

In this experiment, with A_0, A_1, A_2, B_0, B_1, and B_2 unknown parameters, the regenerated RPCs were found to be of slightly higher quality which indicates that there was a little additional distortion error absorbed by scale parameters. With a minimum of five GCPs, an accuracy of 0.8 m in X, 1.2 m in Y and 1.3 m in height has been achieved. The biases in the ground space are listed in table 4.

Table 4: RMS value of ChkPs using different selection of GCPs with 1st order bias correction model

No. of GCPs/ChkPs	RMS of check points coordinate differences (meters)		
	X	Y	Z
5/16	0.8	1.2	1.3
7/14	0.8	1.1	1.5
9/12	0.8	1.2	1.6
13/8	0.2	1.2	1.2
15/6	0.2	1.0	1.2
17/4	0.2	0.9	0.9

4.2.3 Modelling with 2nd order polynomial

To further test the effect of the GCPs distribution and parameters selection ($A_0 \approx A_5$, $B_0 \approx B_5$), seven GCPs were used to calculate the bias coefficients. In this case, one redundant point is available, which will make the calculation more reliable. From table 5, the results generated under the control of seven GCPs show some differences from their counter parts in tables 3 and 4. Results in this test are of slightly lower quality than the former two tests. Consequently, only few GCPs are needed in the bias correction in the image space.

Table 5: RMS value of ChkPs using different selection of GCPs with 2nd order bias correction model

No. of GCPs/ChkPs	RMS of check points coordinate differences (meters)		
	X	Y	Z
7/14	1.2	1.3	2.1
9/12	1.2	1.5	2.2
13/8	0.4	1.3	1.5
15/6	0.3	1.1	1.3
17/4	0.2	1.2	1.0

4.3 Bias-corrected RPCs

The third experiment was to improve the geo-location accuracy of IKONOS stereo-pair in the object space based on the bias corrected RPCs with different bias correction models and different control configurations. In this regard, the bias correction parameters were first estimated by using the LSM with the GCPs, and the bias-corrected RPCs were subsequently obtained through the RPC modification. Afterwards, the geo-location accuracies with the refined RPCs were estimated by calculating the ChkPs biases on the ground through space intersection. Detailed discussions on the result of each correction model are given below.

4.3.1 Modelling with one parameter

The assessment for orientation using one parameter (A_0, B_0, C_0, and D_0) offers a simple way to improve the geo-location accuracy. The results in table 6 indicate that when the shift-bias was removed through RPCs modification with only three GCPs, the accuracy of ground point determination was greatly improved from the 7.2 m to 2.3 m in X, 3.1 m to 1.0 in Y and from 16.7 m to 1.2 m in height. However, additional GCPs contributed to the improvement of the planimetric accuracy. When the 17 GCPs were employed, the overall metric potential was 0.7 m in planimetry and about 1.2 m in height. Figure 7 is a typical example shows both the planimetric and height error based on 3 GCPs. As well, figure 9 indicates that the planimetric and vertical accuracies of the refined RPCs with a single parameter are accurate and stable. Under such an observation, the planimetric accuracy of the refined RPC is around one meter when using 13 to 17 GCPs. On the other hand, the vertical accuracy with 3 GCPs was 1.2 meter with IKONOS data and it remains the same when 17 GCPs were used.

Table 6: RMS value of ChkPs using different selection of GCPs with one parameter bias correction model

No. of GCPs/ChkPs	RMS of check points coordinate differences (meters)		
	X	Y	Z
3/18	2.3	1.0	1.2
5/16	0.9	1.0	1.6
7/14	0.8	0.9	1.7
9/12	0.9	1.0	1.8
13/8	0.3	1.0	1.5
15/6	0.3	0.6	1.5
17/4	0.3	0.6	1.2

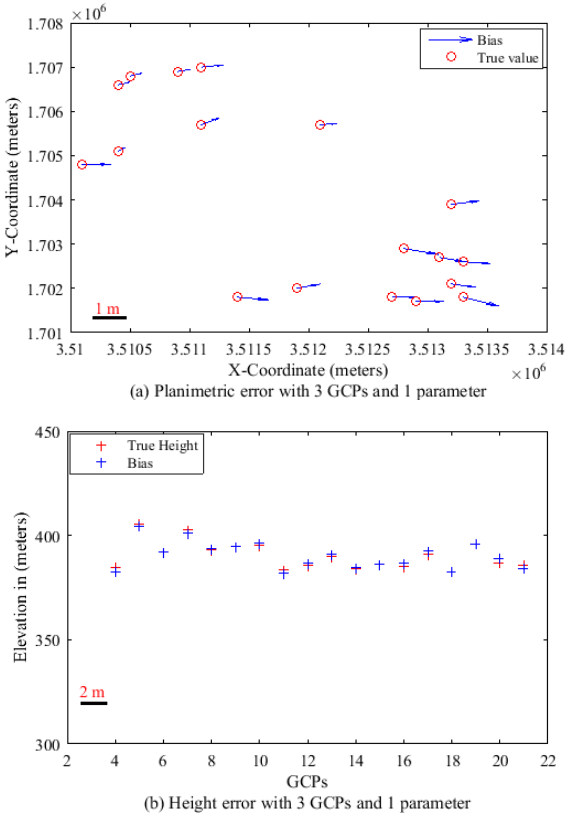

Figure 7: Bias errors of (a) planimetry and (b) height at ChkPs using 3 GCPs and 1 parameter

4.3.2 Modelling with two parameters

To further test the effect of the GCP configuration, five GCPs were used to calculate the eight coefficients, A_0, A_1, B_0, B_1, C_0, C_1, D_0, and D_1. By using these five GCPs, one redundant point is available. From figure 8 and the RMS value on the ChkPs listed in table 7, it is clear that the use of five GCPs could also achieve very good results in bias removing. The RMS values are of the same order of magnitude as in the case of using three GCPs. Figure 9

shows the planimetric and vertical accuracies of the refined RPCs with only two parameters. In essence, 1.4 meter was the observed vertical accuracy when using five GCPs and 0.9 meter was achieved with 17 GCPs, which is not quite significant when compared with the results of the initial case. On the other hand, the planimetric accuracy yields 1.8 meter with 5 GCPs and 1.1 meter with 17 GCPs.

Table 7: RMS value of ChkPs using different selection of GCPs with two parameters bias correction model

No. of GCPs/ChkPs	RMS of check points coordinate differences (meters)		
	X	Y	Z
5/16	1.2	1.4	1.4
7/14	0.6	1.3	1.6
9/12	0.7	1.4	1.7
13/8	0.2	1.3	1.3
15/6	0.2	1.1	1.2
17/4	0.2	1.1	0.9

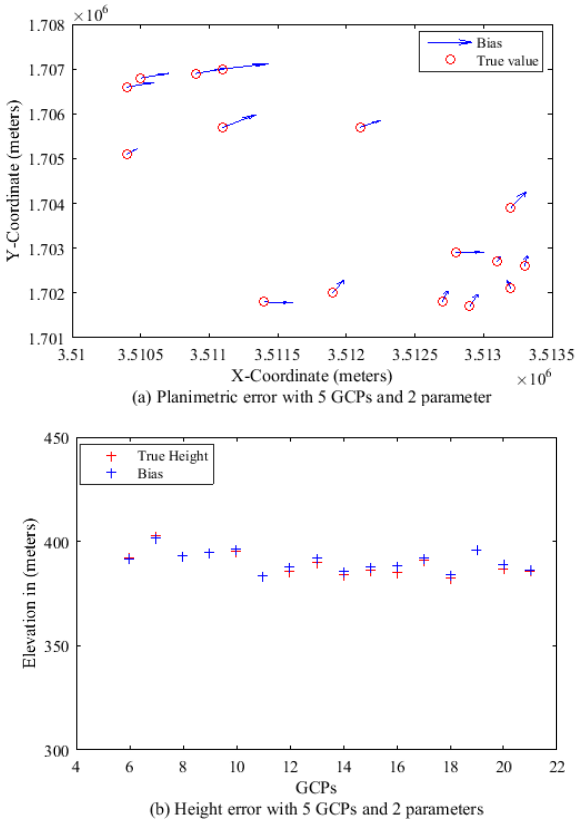

Figure 8: Error vectors in (a) planimetry and (b) height of ChkPs using 5 GCPs and 2 parameters

In the bias corrected RPCs, it was found that the results are getting worse with more parameters (modelling with three and four parameters).

4.4 Bias-corrected object space

The objective is to find out in which domain the bias compensation could achieve a better result with different bias correction models and different control information. For each model in object space, RFM based triangulation (Di et al., 2003; X. Niu et al., 2004) is applied to calculate the ground coordinates (X^{RF}, Y^{RF}, Z^{RF}). Since the GPS coordinates (X^{GPS}, Y^{GPS}, Z^{GPS}) are known, three equations can be established in accordance with the model equations in subsection (2.2.3). Using all available GCPs, over-determined equation systems can be setup to compute the optimal estimates of the transformation parameters by a LSM. The transformation parameters can be used to compute the improved coordinates of other points. ChkPs are used to assess the appropriateness of the models. RMS value of each model is calculated based on differences between RFM derived and known coordinates of the ChkPs.

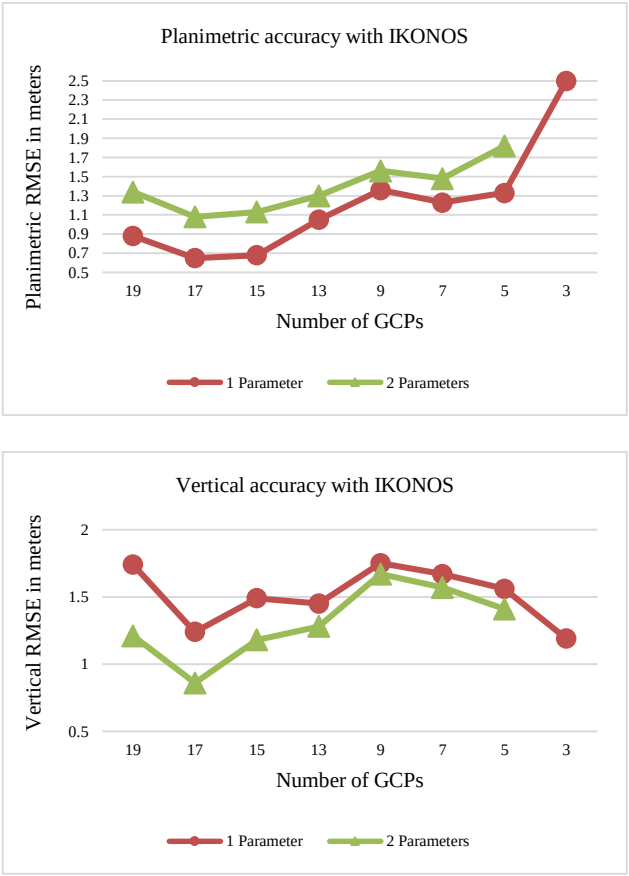

Figure 9: Planimetric and vertical accuracy of object coordinates

The shift parameters (a_0, b_0, c_0) and three additional scale factors (a_1, b_1, c_1) have been applied to correct for non-homogeneous scale distortions. Minimum of two GCPs are required. An affine and a 2nd order polynomial transformation are applied to the second and third models, respectively.

Additional GCPs are then added to improve accuracy. Different combinations of the number and configuration of GCPs are also tested to determine the effectiveness of different distributions. Tables 8, 9 and 10 show improvements in accuracy achieved by the three different models performed in the object space for IKONOS stereo-pair imagery. A discussion of the results of each model is given below.

4.4.1 Modelling with shift and scale

The scale and shift model has additional scaling factors in the coordinate axis directions (a_0, b_0, c_0, a_1, b_1, c_1). The experiment starts with three GCPs and in order to increase redundancy, more GCPs should be used. With nine evenly distributed GCPs, the result is improved. The RMS value is 1.7 m in X, 1.2 m in Y and 1.9 m in height. With 17 GCPs, more consistent and better results were obtained. A RMS value of 1.2 m in X, 0.9 m in Y and 2 m in height were achieved. The RMS values are listed in table 8.

Table 8: RMS value of ChkPs using different selection of GCPs with shift and scale bias correction model

No. of GCPs/ChkPs	RMS of check points coordinate differences (meters)		
	X	Y	Z
3/18	1.9	1.0	4.3
5/16	1.8	1.2	3.3
7/14	1.6	1.1	2.7
9/12	1.7	1.2	1.9
11/10	1.5	1.0	2.1
13/8	1.5	1.2	2.0
15/6	1.4	0.9	2.1
17/4	1.2	0.9	2.0

4.4.2 Modelling with 1st order polynomials

The affine model, 1st order polynomials, offers the capability of considering affinity. However, the additional affine parameters and GCPs can generate an improvement over the result from the scale and shift model. From the RMS values listed in table 9, one can observe that the same accuracy level was achieved with modelling in the bias corrected image space with first order polynomial, see table 4.

Table 9: RMS value of ChkPs using different selection of GCPs with 1st order bias correction model

No. of GCPs/ChkPs	RMS of check points coordinate differences (meters)		
	X	Y	Z
5/16	0.9	1.3	1.5
7/14	0.7	1.1	1.5
9/12	0.8	1.2	1.7
11/10	0.8	1.0	1.8
13/8	0.5	1.2	1.2
15/6	0.4	1.0	1.2
17/4	0.2	0.9	0.9

4.4.3 Modelling with 2nd order polynomials

The addition of the 2nd order parameters requires the use of a larger number of GCPs, at least 10 control points. With 11 GCPs, no significant improvements are found in comparison to the other two models. In general, high-order polynomials are very sensitive and require a large number of GCPs. The 2nd order polynomial model does not exhibit convincing advantages over other models, see table 10.

Table 10: RMS value of ChkPs using different selection of GCPs with 2nd order bias correction model

No. of GCPs/ChkPs	RMS of check points coordinate differences (meters)		
	X	Y	Z
11/10	4.6	2.2	2.9
13/8	2.0	2.2	0.9
15/6	1.3	3.2	0.9
17/4	0.5	1.4	1.1

4.5 3D-Affine model

The 3D affine model transforms the 3D object space to 2D image space for scanners with a narrow AFOV. When modelling with the 3D 1st order polynomial model, 8 coefficient values change for one image (A_0, A_1, A_2, A_3, B_0, B_1, B_2, and B_3), which requires a minimum of 4 points for the space resection. Four equations are derived for each GCP with just three unknowns X, Y and Z. Table 11 summarizes the performances of the first order 3D-Affine model under different evenly distributed GCP and ChkPs combinations. When 5 GCPs are used, the 3D-Affine model produced an overall RMS value of 1.7 m in planimetry and 1.5 m in height. The RMS value reached the lowest RMS value when 17 GCPs were used, RMS values of 1.0 m in planimetry and 1.2 in height.

Table 11: RMS value for ChkPs Using 3D-Affine Model for Stereo Images with 1st order polynomials

No. of GCPs/ChkPs	RMS of check points coordinate differences (meters)		
	X	Y	Z
5/16	1.0	1.4	1.5
7/14	0.8	1.2	1.5
9/12	0.8	1.2	1.6
11/10	0.8	1.0	1.8
13/8	0.5	1.2	1.3
15/6	0.4	1.0	1.4
17/4	0.2	0.9	1.2

When modelling with the 3D 2nd order polynomial model, 14 coefficient values change for one image which requires a minimum of 7 points for the space resection. Table 12 lists the results for different number of GCPs. One can observe that the results are improved as the number of GCPs is increased.

Table 12: RMS value for ChkPs Using 3D-Affine Model for Stereo Images with 2nd order polynomials

No. of GCPs/ChkPs	RMS of check points coordinate differences (meters)		
	X	Y	Z
7/14	3.8	1.7	2.2
9/12	2.7	1.6	2.3
11/10	1.3	1.1	1.9
13/8	1.8	1.4	2.0
15/6	1.1	1.6	1.6
17/4	1.0	1.2	1.1

4.6 DLT model

As new sensors become operational with the new high resolution satellite imagery, their sensor modelling may still not be available immediately. For this reason, during this investigation the capabilities of the existing systems were tested using the DLT model. First, the image space and the ground space coordinates are used to calculate the respective DLT model parameter; L_1, L_2, L_3, L_4, L_5, L_6, L_7, L_8, L_9, L_{10}, and L_{11}. This requires a minimum of 6 GCPs for the space resection. After that, check points were measured on each image for assessing the accuracy of the derived DLT parameters.

Table 13 listed the RMS value of the ChkPs for the IKONOS stereo-pair imagery. The RMS values of the ground residuals were 1.8 m in X, 1.5 m in Y, and 2.1 m in height when 7 GCPs were used. On the other hand, RMS values of 1.2 m in X, 1.0 m in Y, and 1.1 in height were achieved with 17 GCPs. The results can be further improved if the image pixels are corrected for systematic errors.

Table 13: RMS value for ChkPs Using DLT Model for Stereo Images

No. of GCPs/ChkPs	RMS of check points coordinate differences (meters)		
	X	Y	Z
7/14	1.8	1.5	2.1
9/12	1.7	1.7	2.2
11/10	1.6	1.8	2.4
13/8	1.6	1.4	1.5
15/6	1.8	1.4	1.4
17/4	1.2	1.0	1.1

5. Conclusions

Based on the experimental results with IKONOS stereo-pair images, several conclusions were made. The accuracy figures of the 3D-reconstruction using the vendor-supplied RPCs was 7 m in X, 3 m in Y, and 17 m in the Z direction. By applying five bias reduction models with a few number of GCPs, this bias can be compensated to around one meter level of accuracy. The experimentation results show that the accuracies of the used five models are slightly variant. With five GCPs, planimetric and vertical accuracies of better than 1.3 m and 1.6 m respectively, can be obtained using the bias-corrected RPCs and the bias corrected image space approaches. The bias corrected ground space is feasible for RPC refinement in the cases of using shift and scale model and the affine model. Among the simple geometric models, the 1st order 3D polynomial gives accuracies within 1 m in planimetry and 1.5 m in height. On the other hand, the 2nd order 3D polynomial model gives less accuracy figures. Regarding the DLT model, obtained accuracy numbers in X, Y, and Z direction are nearly one meter when using large number of control points.

References

Abdel-Aziz, Y.I. and H. M Karara (1971). Direct linear Transformation from Comparator coordinates into Object space coordinates in close-range Photogrammetry. Proceedings of the Symposium on Close-Range Photogrammetry. Falls Church, VA: American Society of Photogrammetry, pp. 1-18.

Di, K., R. Ma. and R. Li (2003). Rational functions and potential for rigorous sensor model recovery, Photogrammetric Engineering & Remote Sensing, 69(1), 33-41.

Fraser et al., (2006). Sensor orientation via RPCs. ISPRS Journal of Photogrammetry and Remote Sensing, 60(3), 182-194.

Fraser, C., A., T. Ono., S. Akamatsu., S. Hattori. and H. Hasegawa (1999). Geometric characteristics of alternative triangulation models for satellite imagery. Proceedings of 1999 ASPRS Annual Conference, From Image to Information, Oregon, May 17-21.

Fraser, C.S. and H. B. Hanley (2003). Bias compensation in rational functions for IKONOS satellite imagery. Photogrammetric Engineering & Remote Sensing, 69(1), 53-58.

Fraser, C.S. and H. B. Hanley, (2005). Bias compensated RPCs for sensor orientation of high-resolution satellite imagery. Photogrammetric Engineering & Remote Sensing, 71(8), 909-915.

Ghilani, C. D. and P. R. Wolf, (2006). Adjustment Computations: Spatial Data Analysis, Fourth Edition John Wiley & Sons, Inc. ISBN: 978-0-471- 69728-2.

Gong, K. and D. Fritsch (2016). A detailed study about Digital Surface Model generation using high resolution satellite stereo imagery. ISPRS Annals of the Photogrammetry, Remote Sensing and Spatial Information Sciences, Volume III-1.

Grodecki, J. and G. Dial (2003). IKONOS stereo accuracy without ground control, ASPRS Annual Conference Proceedings, Anchorage, Alaska.

Grodecki, J. and G. Dial, (2003). Block adjustment of high-resolution satellite images described by rational polynomials. Photogrammetric Engineering & Remote Sensing, 69(1), 59-68.

Hanley, H.B, and C. S. Fraser (2004). Sensor orientation for high resolution satellite imagery: Further insights into bias compensated RPCs. The International Archives of the Photogrammetry, Remote Sensing and Spatial Information Sciences, 35 Part B1, Istanbul, Turkey.

Hu, Y., V. Tao. and A. Croitor (2004). Understanding the Rational Function Model: Methods and Applications. The International Archives of the Photogrammetry, Remote Sensing and Spatial Information Sciences.

Niu X, et al., (2004). Geometric modelling and photogrammetric processing of high resolution satellite imagery. Mapping and GIS Laboratory, CEEGS, the Ohio State University. Commission IV, WG IV/7

OGC (Open GIS Consortium) (1999). The Open GIS Abstract Specification-Topic 7: The earth imagery Case. http://portal.opengeospatial.org/files/?artifact_id=7467.

Poon, J., C. Fraser., C. Zhang., L. Zhang. and A. Gruen (2005). Quality assessment of Digital Surface Models generated from IKONOS imagery. Photogrammetric Record, 20(110), 162-171.

Singh, G., M. Michel, G., Markus, and A., Shefali, (2008). Improved geometric modelling of space borne push-broom imagery using modified rational polynomial coefficients and the impact on DSM generation. MSc. Thesis, International Institute for Geo-information Science and Earth Observation.

Tao, C., Y. Hu., J. Mercer., S. Schnick. And Y. Zhang (2000). Image rectification using a generic sensor model-rational function model. The International Archives of Photogrammetry and Remote Sensing, 33(B3), 874-881.

Tong X., L. Shijie. and W. Qihao (2010). Bias corrected rational polynomial coefficients for high accuracy geo-positioning of Quick-Bird stereo imagery. ISPRS Journal of Photogrammetry and Remote Sensing 65, 218-226.

Vincent, T. and H. Yong (2000). Image rectification using a generic sensor model – Rational Function Model. International Archives of Photogrammetry and Remote Sensing. XXXIII, Part B3.

Vincent, T. and H. Yong (2002). 3D reconstruction methods based on the Rational Function Model. Photogrammetric Engineering & Remote Sensing, 68(7), 705-714.

Xu Sun., L. Jonathan. and A. Michael (2005). Automatic extraction of Digital Elevation Models from IKONOS in-track stereo images. Department of Civil Engineering, Ryerson University.

Zhen Xiong and Yun Zhang (2009). A generic method for RPC refinement using ground control information. Journal of the American Society for Photogrammetry and Remote Sensing. 75(9), 1083–109.